Available online at www.sciencedirect.com
SCIENCE DIRECT®
Journal of Solid State Chemistry 173 (2003) 114–121
JOURNAL OF SOLID STATE CHEMISTRY
http://elsevier.com/locate/jssc

Trends in the structure and bonding in the layered platinum dioxide and dichalcogenides PtQ_2 (Q = O, S, Se, Te)

D. Dai,[a] H.-J. Koo,[a] M.-H. Whangbo,[a,*] C. Soulard,[b] X. Rocquefelte,[b] and S. Jobic[b,*]

[a] *Department of Chemistry, North Carolina State University, Raleigh, NC 27695-8204, USA*
[b] *Laboratoire de Chimie des Solides, Institut des Matériaux Jean Rouxel, 2 rue de la Houssinière, BP. 32229, 44322 Nantes Cedex 03, France*

Received 25 October 2002; received in revised form 13 January 2003; accepted 31 January 2003

Abstract

The structure and bonding of the layered platinum dioxide and dichalcogenides PtQ_2 (Q = O, S, Se, Te) were analyzed on the basis of electronic band structure calculations using the full potential linearized augmented plane wave method. We examined why the c/a ratio in PtQ_2 is considerably small compared with the value expected from the consideration of closely packed Q atoms (i.e., ~1.40 vs. 1.67), and identified the electronic factor that causes the semiconducting properties in PtO_2 and PtS_2, the semimetallic property in $PtSe_2$, and the metallic property in $PtTe_2$. To a first approximation, the oxidation states of oxygen and platinum in PtO_2 can be regarded as –2 and +4, respectively, but this picture is not applicable to $PtTe_2$. As the ligand Q is changed from O to S to Se to Te, the energy gap between the Pt 5*d* and the ligand *p* levels gradually decreases, so that the ionic character of the Pt–Q bonding in PtQ_2 is gradually diminished.

Keywords: Layered platinum dioxide; Layered platinum dichalcogenides; Structure and bonding; Electronic band structures

1. Introduction

Most transition metal oxides adopt three-dimensional (3D) structures, and low-dimensional oxide structures are usually stabilized by separating highly charged O^{2-} anions with counter cations (e.g., Na_xCoO_2, $K_{0.3}MoO_3$, etc.) and employing transition elements of high oxidation state (e.g., MoO_3, V_2O_5, etc.). In contrast, transition metal sulfides and selenides exhibit layered structures for early transition elements, and 3D structures for late transition metal elements [1,2]. The tendency to adopt low-dimensional structures is further enhanced in transition metal tellurides [3,4]. Thus, low-dimensional chalcogenides are stabilized in the absence of counter cations and with transition elements of low oxidation state [5]. From this point of view, the CdI_2-type layered compounds PtQ_2 (Q = O, S, Se, Te) are unusual. Each PtQ_2 layer is made up of edge-sharing PtQ_6 octahedra (Fig. 1a), and the 3D structure of PtQ_2 is obtained by stacking PtQ_2 layers (Fig. 1b). The interactions between adjacent MQ_2 layers in layered transition metal dichalcogenides MQ_2 are frequently described as van der Waals (VDW) interactions. Given the space group $P\bar{3}ml$, the crystal structure of PtQ_2 is completely determined by specifying three parameters, i.e., the unit-cell parameters a and c as well as the z-coordinate of the Q atom position (Table 1).

The layered PtQ_2 compounds raise a number of interesting questions about their structures and bonding. They have a c/a ratio of approximately 1.4, which is significantly smaller than the value (i.e., 1.67) expected from the consideration of an ideal hexagonal close packing of Q atoms. So far it is not understood how this observation is related to the electronic structure of PtQ_2. The c-parameter of PtQ_2 is given by $c = d_L + d_V$, where d_L is the thickness of a single PtQ_2 layer, and d_V is that of the VDW gap (Fig. 1b). It is noted that $d_L = d_V$ when $z = 0.25$, $d_L < d_V$ when $z < 0.25$, and $d_L > d_V$ when $z > 0.25$. So far there are only brief reports on the crystal structures of PtO_2 (6) and PtQ_2 (Q = S, Se, Te) [7]. In the crystal structure determination of PtO_2, it was assumed that $z = 0.25$ [6]. It was reported [7] that the z-coordinate of PtS_2 is considerably smaller than 0.25, but those of $PtSe_2$ and $PtTe_2$ are close to 0.25 (Table 1). The electronic band structures of PtQ_2 (Q = S, Se, Te) were examined some years ago by Guo and Liang [8]

*Corresponding authors. Fax: +1-919-515-7832.
E-mail addresses: mike_whangbo@ncsu.edu (M.-H. Whangbo), stephane.jobic@cnrs-imn.fr (S. Jobic).

0022-4596/03/$ - see front matter © 2003 Elsevier Science (USA). All rights reserved.
doi:10.1016/S0022-4596(03)00100-2

using the LMTO-ASA method [9,10] and the reported crystal structures [7]. This study showed that PtS_2 is a semiconductor, $PtSe_2$ is a semimetal, and $PtTe_2$ is a metal in agreement with experiment [11–13]. However, the electronic and structural factors causing this variation of the electrical property have not been identified. Furthermore, it is puzzling that the experimentally determined z-coordinates of Q do not show a gradual change as a function of Q. Thus it is important to determine the optimum z-values on the basis of first principles electronic band structure calculations. This is also important in understanding the low c/a ratio of the PtQ_2 compounds.

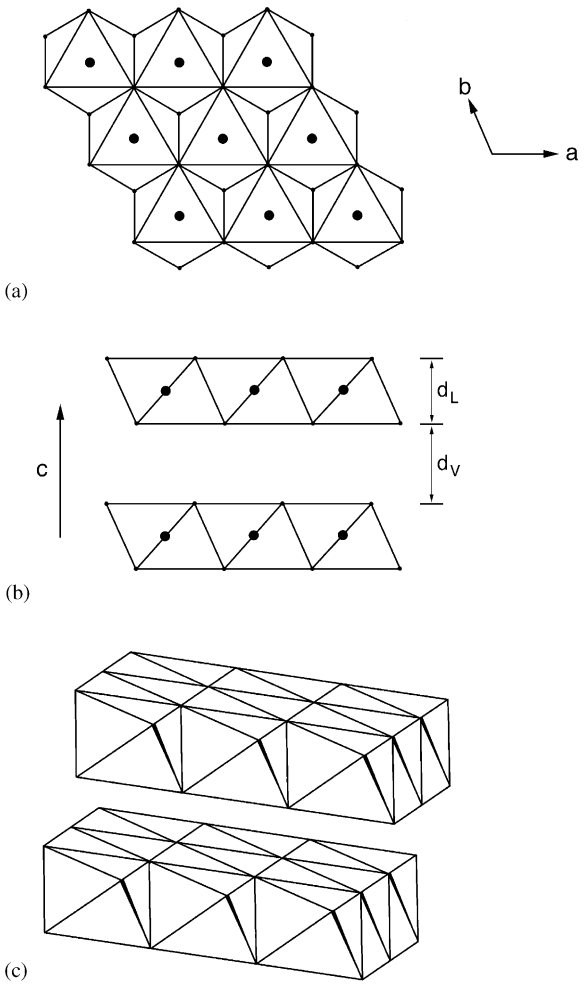

Fig. 1. (a) Schematic projection view of a single PtQ_2 layer along the c-direction. (b) Schematic projection view of adjacent PtQ_2 layers along the direction perpendicular to the c-direction. (c) Perspective view of two PtQ_2 layers.

The study of the electronic structures of the PtQ_2 compounds provides an excellent opportunity to examine the conceptual pictures employed in describing the electronic properties of transition metal compounds ML_n (M = transition metal, L = main group element). In predicting the orbital character of the highest occupied and lowest unoccupied levels (i.e., the frontier energy levels) of ML_n on a qualitative level, the ionic electron counting (IEC) scheme is frequently employed. When L is oxygen, chalcogen and halogen atoms, this scheme assumes that L adopts the inert gas electron configuration and the remaining valence electrons of ML_n occupy the d-block levels of transition metals. This prediction is correct when L is more electronegative than M, but becomes erroneous otherwise [14–16]. For example, the IEC scheme predicts that the square planar anion $[AuI_4]^-$ of $[N(n\text{-}Bu)_4]AuI_4$ has an Au^{3+} ion, and the linear anion $[AuI_2]^-$ of $[N(n\text{-}Bu)_4]AuI_2$ has an Au^+ ion [17]. Likewise, the square planar $AuTe_4$ units in $(Et_4N)_4Au_2Te_{12}$ [18], $(Et_4N)_4KAuAs_4Te_8$ [19], and $(Et_4N)_4AuTe_7$ [20] are often considered to have an Au^{3+} ion. By analogy with the chemistry of the Ni^{2+} (d^8) ions, the Au^{3+} (d^8) picture provides a ready rationalization for the square planar structure of the AuI_4 and $AuTe_4$ units. However, both electronic structure calculations [14,19] and X-ray photoelectron spectroscopy [17] studies show that they contain Au^+ (d^{10}) ions, i.e., all their d-block levels are filled. In essence, the IEC scheme assumes that the d orbital of M lies higher in energy than the valence p orbital of L (= oxygen, chalcogen, halogen). The M–L bond in ML_n reduces ionic character and enhances covalent character as the energy difference between the metal d and the ligand p orbitals is diminished [21]. On going down the rows within a family of the main group elements L, the electronegativity decreases, and the

Table 1
Structural parameters defining the crystal structures of the layered PtQ_2 (Q = O, S, Se, Te)[a]

	a (Å)	c (Å)	c/a	z	
PtO_2[b]	3.100(2)	4.161(3)	1.34	0.25	(0.2291)[c]
PtS_2[d]	3.5432	5.0388	1.42	0.227 ± 0.010	(0.2413)[c]
$PtSe_2$[d]	3.7278	5.0813	1.36	0.255 ± 0.003	(0.2466)[c]
$PtTe_2$[d]	4.0259	5.2209	1.30	0.254 ± 0.005	(0.2603)[c]

[a] Space group: $P\bar{3}m1$.
[b] Ref. [9].
[c] The numbers in parentheses are the values optimized by FP-LAPW calculations.
[d] Ref. [7].

valence p orbital is raised in energy and becomes more diffuse. Thus, for compounds ML_n of a late transition metal M with fourth-row main group elements L, the metal d orbital level may become very close to, or even slightly lower than, the ligand p level. For such systems, it is necessary to use a modified electron-counting scheme to correctly predict the nature of their frontier orbitals [15,16]. Given a series of isoelectronic and isostructural compounds ML_n of a late transition metal M, it is possible that the IEC scheme might be adequate for the member with the first-row element L, but not for the member with the fourth-row element L. It is important to examine how the structure and bonding of such a series evolve as a function of the ligand L. The layered platinum dioxide and dichalcogenides PtQ_2 (Q = O, S, Se, Te) are a representative series with which to probe this question.

In the present work we examine the electronic structures of PtQ_2 using the full potential linearized augmented plane wave (FP-LAPW) method [22]. We then analyze the trends in the structure and bonding of PtQ_2 to find why their c/a ratio is small. Finally, we investigate the primary electronic factor responsible for why PtO_2 and PtS_2 are semiconductors, $PtSe_2$ is a semimetal, and $PtTe_2$ is a metal.

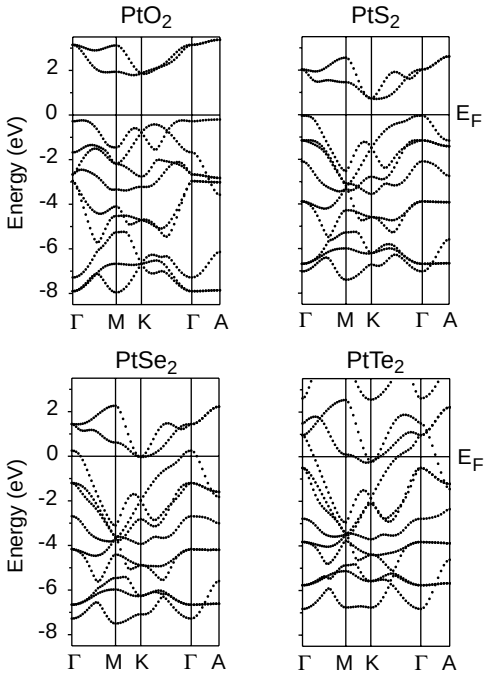

Fig. 2. Band dispersion relations of (a) PtO_2, (b) PtS_2, (c) $PtSe_2$ and (d) $PtTe_2$ obtained from FP-LAPW calculations. $\Gamma = (0,0,0)$, $M = (a^*/2,0,0)$, $K = (a^*/3,b^*/3,0)$, and $A = (0,0,c^*/2)$.

2. Calculations

We carried out FP-LAPW calculations for PtQ_2 (Q = O, S, Se, Te) using the WIEN2k program package [22] within the generalized gradient approximation [23] for the exchange-correlation energy. We employed the muffin-tin radii of 2.32 a.u. for Pt, 1.48 a.u. for O, 2.06 a.u. for S, 2.33 a.u. for Se, and 2.61 a.u. for Te (Our study shows no noticeable variation in the results with muffin-tin radii). The basis set cut-off parameters were $G_{max} = 14$ and $R_{mt} \cdot K_{max} = 7$. Integrations over the irreducible wedge of the Brillouin zone were performed using a 2500 k-point regular mesh. In our FP-LAPW calculations, the total electronic energy of each PtQ_2 was determined as a function of the z-coordinate of Q (while keeping the cell parameters a and c fixed at the experimental values) to obtain its optimum value. We also examined the electronic structures of PtQ_2 using the extended Hückel tight binding (EHTB) method [24,25] to analyze the interlayer orbital interactions that are critical for the presence and absence of a band gap in PtQ_2.

The optimized z values of Q for PtQ_2 calculated from energy minimization are listed in Table 1. The band dispersion relations calculated for the optimized structures of PtQ_2 are shown in Fig. 2a–d, and the corresponding plots of the total and partial density of states in Fig. 3a–d. With the local coordinate z-axis taken along the c-direction, the Pt $5d$ orbitals can be grouped into d_{z^2}, (d_{xz}, d_{yz}) and $(d_{x^2-y^2}, d_{xy})$ while the p orbitals of Q into p_z and (p_x, p_y). The orbital compositions of the energy bands of PtQ_2 (Q = O, S, Se, Te) are presented in Figs. 4–7 in terms of fat band representations.

Figs. 2 and 3 show that the conduction and valence bands are well separated by a band gap in PtS_2, overlap very weakly in $PtSe_2$, and overlap significantly in $PtTe_2$. These results are quite similar in nature to those reported by Guo and Liang [8], and those found for TiQ_2 (Q = S, Se, Te) series [26] in which the valence and conduction bands are represented by the p- and d-block bands, respectively.

3. Structural trends and their implications

Our calculations show that the z value of Q is considerably smaller than 0.25 for Q = O, gradually increases as Q moves to S to Se to Te, and becomes larger than 0.25 for Q = Te (Table 1). Table 2 lists the d_L and d_V values of PtQ_2 (Q = O, S, Se, Te) determined from their optimized structures. As expected from the optimized z values, d_L is smaller than d_V in PtO_2 and PtS_2, but close to d_V in $PtSe_2$, and larger than d_V in $PtTe_2$. Table 2 also lists the shortest nonbonded $Q \cdots Q$ distance within a Q-atom sheet (D_{sheet}, i.e., the a-parameter), that between the two Q-atom sheets of a PtQ_2 layer (D_{intra}), and that between the two adjacent

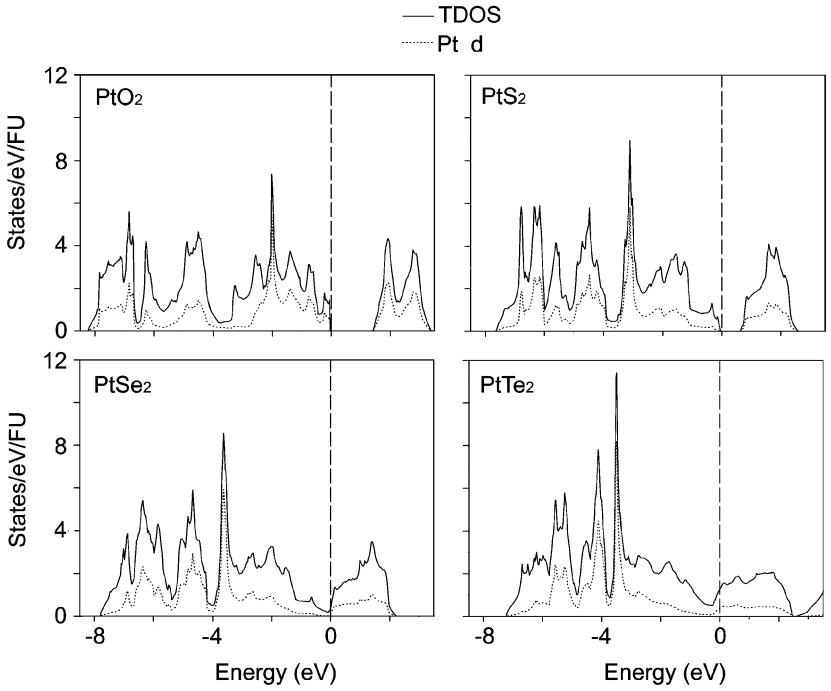

Fig. 3. Plots of the total density of states (TDOS) and the Pt 5*d* orbital contributions to the TDOS obtained by FP-LAPW calculations: (a) PtO_2, (b) PtS_2, (c) $PtSe_2$ and (d) $PtTe_2$.

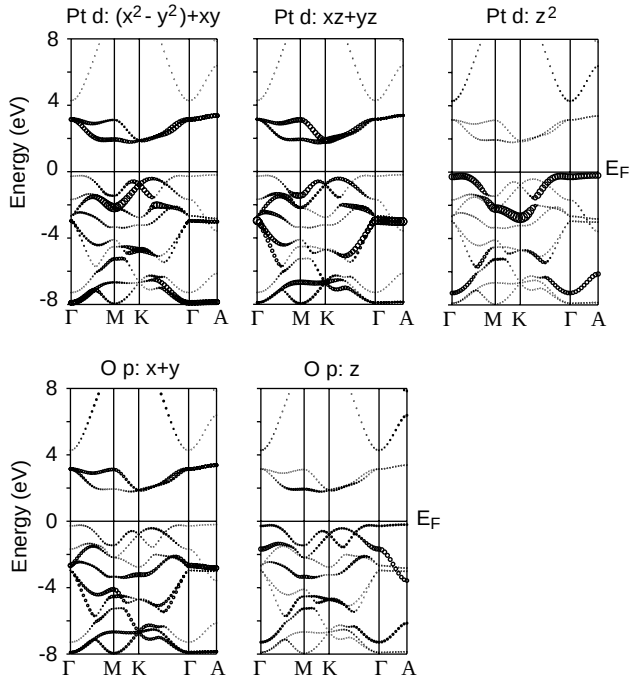

Fig. 4. Band dispersion relations of PtO_2 with fat band representations for the $5d_{z^2}$ orbital of Pt, the $5d_{x^2-y^2}$ and $5d_{xy}$ orbitals of Pt, the $5d_{xz}$ and $5d_{yz}$ orbitals of Pt, the $2p_x$ and $2p_y$ orbitals of O, and the $2p_z$ orbital of O.

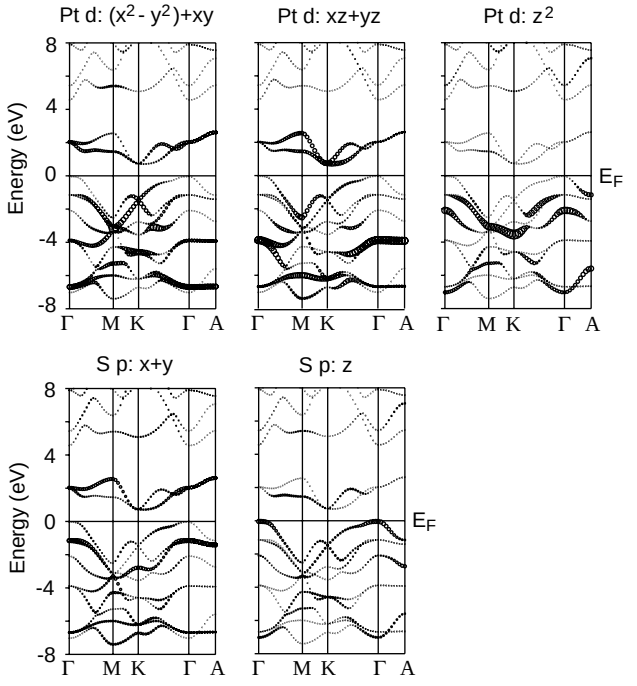

Fig. 5. Band dispersion relations of PtS_2 with fat band representations for the $5d_{z^2}$ orbital of Pt, the $5d_{x^2-y^2}$ and $5d_{xy}$ orbitals of Pt, the $5d_{xz}$ and $5d_{yz}$ orbitals of Pt, the $3p_x$ and $3p_y$ orbitals of S, and the $3p_z$ orbital of S.

Q-atom sheets of two neighboring PtQ_2 layers (D_{inter}). It is noted that $D_{sheet} > D_{intra}$ and $D_{sheet} > D_{inter}$ for each PtQ_2 (Q = O, S, Se, Te). Since $D_{sheet} > D_{intra}$, the PtQ_6 octahedra are squashed along the *c*-direction. Thus, if the three-fold rotational axis of each PtQ_6 octahedron perpendicular to the PtQ_2 layer may be taken as the

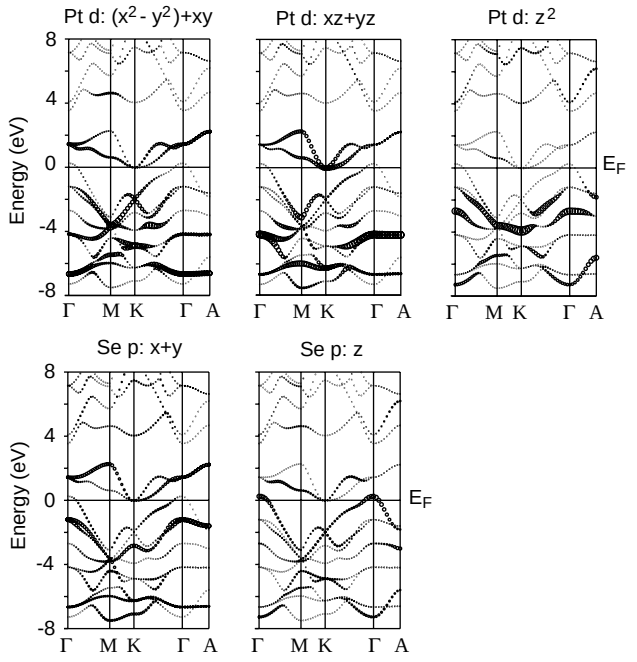

Fig. 6. Band dispersion relations of $PtSe_2$ with fat band representations for the $5d_{z^2}$ orbital of Pt, the $5d_{x^2-y^2}$ and $5d_{xy}$ orbitals of Pt, the $5d_{xz}$ and $5d_{yz}$ orbitals of Pt, the $4p_x$ and $4p_y$ orbitals of Se, and the $4p_z$ orbital of Se.

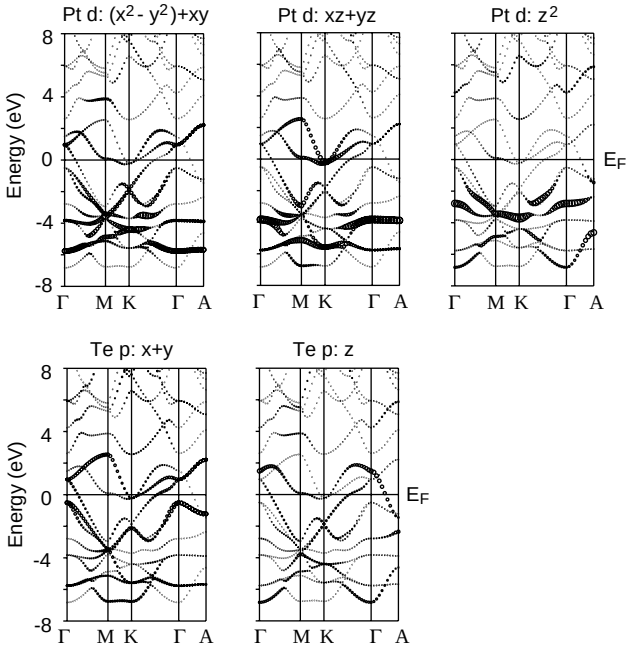

Fig. 7. Band dispersion relations of $PtTe_2$ with fat band representations for the $5d_{z^2}$ orbital of Pt, the $5d_{x^2-y^2}$ and $5d_{xy}$ orbitals of Pt, the $5d_{xz}$ and $5d_{yz}$ orbitals of Pt, the $5p_x$ and $5p_y$ orbitals of Te, and the $5p_z$ orbital of Te.

local z-axis, then the $\angle Q$–Pt–Q angle taken within each PtQ_3 trigonal pyramid with its three-fold rotational axes aligned along the local z-axis is significantly larger than 90°. These $\angle Q$–Pt–Q angles are nearly identical for all Q (Table 2), so that the D_{sheet}/D_{intra} ratios are nearly identical for all Q.

For an ideal close-packed structure of Q atoms, $D_{sheet} = D_{intra} = D_{inter}$, and the c/a ratio is 1.67. Thus, to understand why the c/a ratio is small ($\sim$1.40) in PtQ_2 (Q = O, S, Se, Te), it is necessary to probe why $D_{sheet} > D_{intra}$, D_{inter} in PtQ_2. This can be understood by considering the "overlap repulsion" between the filled np_x, np_y and np_z orbitals of Q. The net result of orbital interaction between two filled orbitals is destabilization and the extent of this destabilization increases with increasing the overlap between the orbitals [21]. The overlap repulsion between the filled np_x orbitals of Q, and that between filled np_y orbitals of Q within each Q-atom sheet should be much stronger than that between the filled np_z orbitals of Q between adjacent Q-atom sheets, because the np_z orbitals between adjacent Q-atom sheets are not coplanar whereas the np_x and np_y orbitals of Q within each Q-atom sheet are coplanar. The most antibonding combinations of the np_x and np_y orbitals within each PtQ_2 sheet are depicted in Fig. 8, and that of the np_z orbitals of Q between adjacent Q-atom sheets in Fig. 9. To reduce the overlap repulsion resulting from the filled np_x and np_y orbitals, each PtQ_6 octahedron should be squashed along the c-direction thereby increasing the a-parameter and hence reducing the c/a ratio. A similar reasoning explained the square planar to rectangular distortion in transition-metal compounds of edge-sharing square planar units MX_4 [27]. The c/a ratio is particularly small for PtQ_2 because the Pt–Q distance is small; the Pt–O distance is about the same as the VDW distance (i.e., 2.028 vs. 2.025 Å), but the Pt–Q (Q = S, Se, Te) distances are smaller than the VDW distances (i.e., 2.380 vs. 2.475 Å for Pt–S, 2.490 vs. 2.625 Å for Pt–Se, and 2.693 vs. 2.825 Å for Pt–Te). For any CdI_2 structure MQ_2 compound (M = transition element), a lower c/a ratio is expected for late transition metals than for early transition metal elements because the M–Q distance is shorter for late transition metals.

The VDW distances of the $Q\cdots Q$ contacts (D_{vdw}) are approximately 2.80, 3.70, 4.00 and 4.20 Å for Q = O, S, Se and Te, respectively. Thus the D_{inter}/D_{vdw} ratio is 1.03, 0.90, 0.84 and 0.78 for Q = O, S, Se and Te, respectively. The D_{inter} is nearly the same as the D_{vdw} in PtO_2, so it would be reasonable to consider the interlayer interactions as VDW interactions for PtO_2. Furthermore, the Pt 5d orbital character is strong in the conduction bands of PtO_2 (Figs. 3a and 4), which are the e_g-block bands. To a first approximation, therefore, one might describe the oxidation states of oxygen and platinum in PtO_2 as –2 and +4, respectively, so the d-electron count of Pt in PtO_2 would be close to d^6. This description is what the IEC scheme predicts, and can be rationalized by considering that the Pt 5d level lies higher in energy than the O 2p level (Fig. 10a). The latter

Table 2
Values of d_L, d_V and the shortest nonbonded $Q\cdots Q$ distances in the optimized structures of PtQ_2 (Q=O, S, Se, Te)

	d_L (Å)	d_V (Å)	$Q\cdots Q$ (Å)			∠ Q–Pt–Q (deg)[d]
			D_{sheet}[a]	D_{intra}[b]	D_{inter}[c]	
PtO_2	1.907	2.254	3.100	2.615	2.879	99.7
PtS_2	2.432	2.607	3.543	3.178	3.314	96.2
$PtSe_2$	2.506	2.575	3.728	3.303	3.356	96.9
$PtTe_2$	2.718	2.503	4.026	3.576	3.415	96.8

[a] Within a Q-atom sheet.
[b] Between the two Q-atom sheets of a PtQ_2 layer.
[c] Between the two adjacent Q-atom sheets of two neighboring PtQ_2 layers.
[d] Taken from each PtQ_3 pyramid with its three-fold rotational axis aligned along the local z-axis.

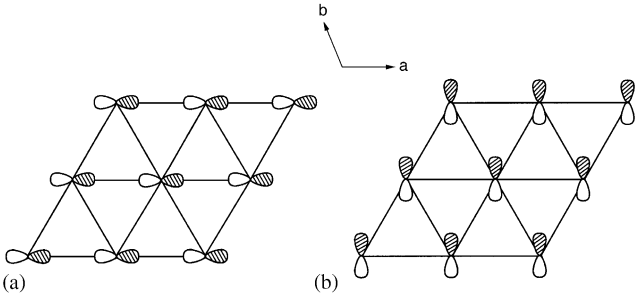

Fig. 8. Schematic representations of the ligand p_x and p_y orbital arrangements in the most sigma antibonding level within each PtQ_2 sheet: (a) p_x and (b) p_y. These arrangements occur for $k_x = k_y = 0$.

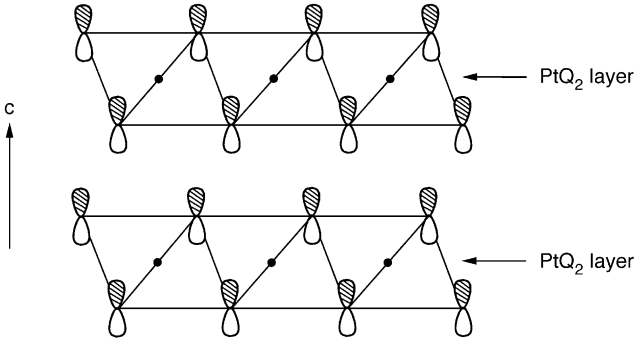

Fig. 9. Schematic representation of the ligand p_z orbital arrangements in the most sigma antibonding level σ_z^* found in the electronic band structure of PtQ_2, which occurs at the Γ point.

induces ionic character into the Pt–O bond [21]. Furthermore, in the antibonding levels ψ_- that form the major orbital character of the e_g-block bands of PtO_2, the Pt 5d contributes more than the O 2p orbital. This explains why the Pt d-orbital character is strong in the conduction bands of PtO_2. In contrast to the case of PtO_2, the D_{inter} is quite shorter than the D_{vdw} in $PtTe_2$ (i.e., $D_{inter}/D_{vdw} = 0.78$). Therefore, it would not be accurate to regard the interlayer interactions in $PtTe_2$ as VDW interactions. We note that the shortest interlayer Te$\cdots$Te distance (3.415 Å for $z = 0.2603$, and 3.464 Å for $z = 0.254$, Table 1) in $PtTe_2$ is comparable to the shortest interchain Te$\cdots$Te distance (3.472 Å) in trigonal tellurium [28], the shortest interlayer Te$\cdots$Te distance (3.469 Å) in monoclinic tellurium [29], and the interlayer layer Te$\cdots$Te distances in the tellurides of late transition elements $IrTe_2$ (3.498 Å) [30] and $NiTe_2$ (3.455 Å) [31], for which the oxidation states of Te are considered to be –1.5 and –1, respectively. Thus it would be appropriate to consider that the tellurium of $PtTe_2$ has the oxidation state close to −1–0 rather than to –2. Then the oxidation state of platinum in $PtTe_2$ would be much closer to +2–0 rather than to +4, and the d-electron count of Pt in $PtTe_2$ would be close to d^8–d^{10}. This reasoning is consistent with the observation that a high oxidation state is difficult to achieve for a transition metal element

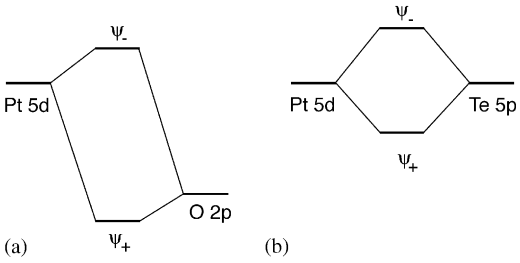

Fig. 10. Orbital interactions between the Pt 5d and the valence p orbitals of Q in PtQ_2: (a) PtO_2 and (b) $PtTe_2$.

when going from the left to the right and from the top to the bottom of the periodic table. This also implies that the Pt 5d orbital character should be weak above the Fermi level. Figs. 3d and 7 show that the latter is indeed the case (see the next section for further discussion). Thus the bonding picture for PtO_2 developed by the IEC scheme is not applicable to $PtTe_2$. As the ligand Q varies from O to S to Se to Te, the np orbital of Q is gradually raised in energy such that the Te 5p level becomes close to the Pt 5d level (Fig. 10b). Thus the ionic character of the orbital interaction between the Q np and Pt 5d levels is continuously reduced as Q varies from O to S to Se to Te.

4. Interlayer orbital interactions and band gap

The inspection of Figs. 4–7 shows that the electronic structures of PtQ_2 vary gradually as Q moves from O to S to Se to Te. In PtO_2 the bottom of the conduction bands are well separated from the highest occupied band level. The bottom level of the conduction bands (hereafter referred to as the ψ_b level) in PtO_2 occurs at the K point, and its major orbital contribution comes from the Pt $5d_{xz}$ and $5d_{yz}$ orbitals (Fig. 4). The top of the valence bands in PtO_2 occurs at the Γ point, and its major orbital contribution comes from the Pt $5d_{z^2}$ orbital. The ψ_b levels of PtS_2, $PtSe_2$ and $PtTe_2$ are very similar in orbital character to that in PtO_2, and its bottom lies at the K point. The top of the valence bands in PtS_2 and $PtSe_2$ occurs at the Γ point, and its major orbital character is given by the most sigma antibonding combinations of the ligand p_z orbitals (hereafter referred to as σ_z^*), as depicted in Fig. 9. Note that the σ_z^* level occurs at the Γ point well below the Fermi level in PtO_2 (Fig. 4), becomes the valence band top but lies below the ψ_b level in PtS_2 (Fig. 5), slightly above the ψ_b level in $PtSe_2$ (Fig. 6), and well above the ψ_b level in $PtTe_2$ (Fig. 7). The analysis of the σ_z^* and ψ_b levels of PtQ_2 in terms of EHTB calculations reveal that these levels vary as a function of Q as summarized in Fig. 11. Namely, the valence and conduction bands do not overlap in PtO_2 and PtS_2, overlap slightly in $PtSe_2$, and overlap strongly in $PtTe_2$. This explains why PtO_2 and PtS_2 are semiconductors, $PtSe_2$ is a semimetal, and $PtTe_2$ is a metal.

It is straightforward to understand why the σ_z^* and ψ_b levels depend on Q as shown in Fig. 11. The O $2p$ orbital lies low in energy and the sigma antibonding interactions between the O $2p$ orbitals in the σ_z^* level are weak because the O $2p$ orbital is contracted. Consequently, the σ_z^* level lies much lower in energy than the ψ_b level in PtO_2. As the ligand Q moves from O to S to Se to Te, the valence p orbital of Q is raised in energy and becomes more diffuse in orbital extension so that the sigma antibonding interactions in the σ_z^* level become stronger. Therefore, the σ_z^* level is continuously raised in energy as the ligand Q varies from O to S to Se to Te. On the other hand, the ψ_b level does not change strongly as a function of Q because it has Pt $5d$ orbital contributions.

There are two reasons why the Pt $5d$ orbital character is weak above the Fermi level in $PtTe_2$. One is that the Te $5p$ level is close to the Pt $5d$ level (Fig. 10b). Thus in the antibonding level ψ_- that form the major orbital character of the e_g-block bands of $PtTe_2$, the Pt $5d$ and the Te $5p$ orbitals contribute almost equally thereby enhancing the covalent character in the Pt–Te bond [21]. The other reason is that the $5p_z$ orbital character of Te is high in the conduction bands of $PtTe_2$ because the σ_z^* level is raised well above the ψ_b level and the Fermi level.

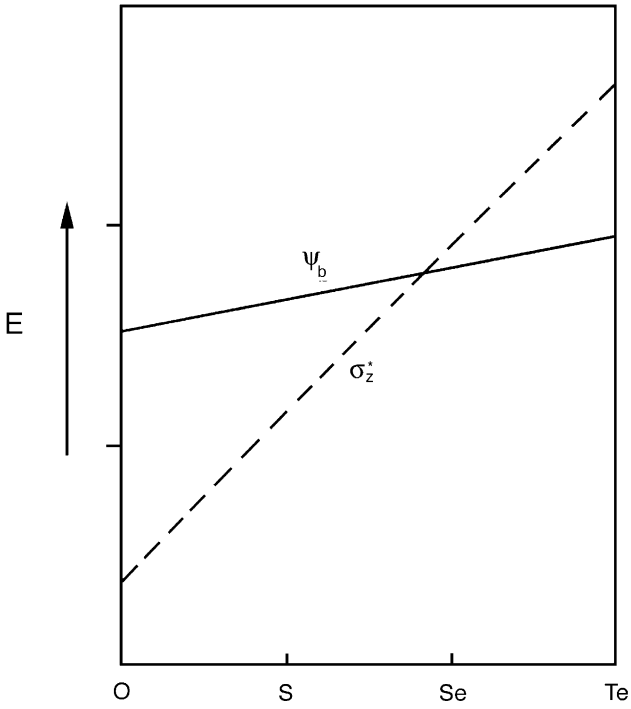

Fig. 11. Variation of the most sigma antibonding level σ_z^* of the ligand p_z orbitals and the bottom level ψ_b of the e_g-block bands in PtQ_2 as a function of Q. Each interval on the energy axis represents 5 eV.

The σ_z^* level is antibonding between the adjacent sheets of Te-atoms between neighboring $PtTe_2$ layers. Such a sigma antibonding character is present in the energy levels lying above the Fermi level. Therefore, the absence of electrons in these levels reduces the extent of antibonding, and hence effectively strengthens the bonding, between adjacent $PtTe_2$ layers. This leads to the reduction of the VDW gap distance d_V in $PtTe_2$. This also explains why short interlayer Te···Te contacts in CdI_2-type layered transition-metal ditellurides have slightly positive overlap populations [32].

In addition to the overlap repulsion effect (in other words, the steric effect), the c/a ratio of PtQ_2 can also be reduced when the interlayer $Q\cdots Q$ contacts become shorter as a consequence of electron removal from the np_z orbital bands of Q. Both factors are at work in $PtTe_2$ ($c/a = 1.30$) and, to a lesser extent, in $PtSe_2$ ($c/a = 1.36$). Only the overlap repulsion effect is operative in PtS_2 ($c/a = 1.42$) and PtO_2 ($c/a = 1.34$).

5. Concluding remarks

Our calculations show that the z value of Q in PtQ_2 varies gradually as a function of Q. It is considerably smaller than 0.25 for $Q = O$, is gradually increased as Q moves to S to Se to Te, and becomes larger than 0.25 for $Q = Te$ (Table 1). To a first approximation, the

oxidation states of oxygen and platinum in PtO_2 can be regarded as –2 and +4, respectively. This picture cannot be extended to $PtTe_2$ because its electronic structure is better described by supposing an oxidation state between +2 and 0 for Pt, i.e., the Pt–Te bond possesses a strong covalent character. The small c/a ratio in PtQ_2 reflects the fact that the overlap repulsion between filled np orbitals of Q is much stronger within each Q-atom sheet than between adjacent Q-atom sheets. As the ligand Q is changed from O to S to Se to Te, the energy gap between the ligand p and the metal $5d$ level gradually decreases (Fig. 10), so that the ionic character of the Pt–Q bond in PtQ_2 is gradually lost. The crucial electronic factor inducing the semiconducting, semimetallic or metallic character in PtQ_2 (Q=O, S, Se, Te) is the interlayer sigma antibonding orbital interactions associated with the valence p_z orbitals of Q (Figs. 9 and 11).

Acknowledgments

Work at North Carolina State University was supported by the Office of Basic Energy Sciences, Division of Materials Sciences, US Department of Energy, under Grant DE-FG02-86ER45259. The authors are grateful to North Carolina Supercomputer Center for the generous computer time.

References

[1] J. Rouxel, Comments Inorg. Chem. 14 (1993) 207.
[2] S. Jobic, P. Deniard, R. Brec, J. Rouxel, M.G.B. Dreaw, W.I.F. David, J. Solid State Chem. 89 (1990) 315.
[3] S. Jobic, R. Brec, J. Rouxel, J. Alloys Compds. 178 (1992) 253.
[4] S. Jobic, R. Brec, J. Rouxel, J. Solid State Chem. 96 (1992) 169.
[5] J. Rouxel, Adv. Chem. 499 (1992) 88.
[6] H.R. Hoekstra, S. Siegel, F.X. Gallagher, Adv. Chem. 98 (1971) 39.
[7] S. Furuseth, K. Selte, A. Kjekshus, Acta Chem. Scand. 19 (1965) 257.
[8] G.Y. Guo, W.Y. Liang, J. Phys. C: Solid State Phys. 19 (1986) 995.
[9] O.K. Andersen, Phys. Rev. B 12 (1975) 3060.
[10] H.L. Skriver, Phys. Rev. B 15 (1977) 1894.
[11] S. Soled, A. Wold, O. Gorochov, Mater. Res. Bull. 11 (1976) 927.
[12] G. Kliche, J. Solid State Chem. 56 (1985) 26.
[13] J. Guggenheim, F. Hulliger, J. Muller, Helv. Phys. Acta 34 (1961) 408.
[14] J.A. Paradis, M.-H. Whangbo, R.V. Kasowski, New J. Chem. 17 (1993) 525.
[15] K.-S. Lee, H.-J. Koo, D. Dai, J. Ren, M.-H. Whangbo, Inorg. Chem. 38 (1999) 340.
[16] K.-S. Lee, H.-J. Koo, J. Ren, M.-H. Whangbo, J. Solid State Chem. 147 (1999) 11.
[17] H. Kitagawa, N. Kojima, T. Nakajima, J. Chem. Soc. Dalton Trans. (1991) 3121.
[18] S.S. Dhingra, R.C. Haushalter, Inorg. Chem. 33 (1994) 2735.
[19] C. Wang, R.C. Haushalter, M.-H. Whangbo, Inorg. Chem. 37 (1998) 6096.
[20] M.A. Ansari, J.C. Bollinger, J.A. Ibers, J. Am. Chem. Soc. 115 (1993) 3838.
[21] T.A. Albright, J.K. Burdett, M.-H. Whangbo, Orbital Interactions in Chemistry, Wiley, New York, 1985 (Chapter 2).
[22] P. Blaha, K. Schwarz, G. Madsen, D. Kvasnicka, J. Luitz, WIEN2k, An Augmented Plane Wave + Local Orbitals Program for Calculating Crystal Properties, Karlheinz Schwarz, Techn. Universität Wien, Austria, 2001. ISBN 3-9501031-1-2. See also: http://www.wien2k.at/
[23] J.P. Perdew, S. Burke, M. Ernzerhof, Phys. Rev. Lett. 77 (1996) 3865.
[24] M.-H. Whangbo, R. Hoffmann, J. Am. Chem. Soc. 100 (1978) 6093.
[25] J. Ren, W. Liang, M.-H. Whangbo (Eds.), Crystal and Electronic Structure Analysis Using CAESAR, 1998.
[26] E. Canadell, S. Jobic, R. Brec, J. Rouxel, M.-H. Whangbo, J. Solid State Chem. 98 (1992) 59.
[27] N. Gupta, D.-K. Seo, M.-H. Whangbo, S. Jobic, J. Rouxel, R. Brec, J. Solid State Chem. 128 (1997) 181.
[28] C. Adenis, V. Langer, O. Lindqvist, Acta Crystallogr. C 45 (1989) 941.
[29] K. Aoki, O. Shimomura, S. Minomura, J. Phys. Soc. Jpn. 48 (1980) 551.
[30] S. Jobic, P. Deniard, R. Brec, J. Rouxel, Z. Anorg. Allg. Chem. 598/599 (1991) 199.
[31] W. Bensch, W. Heid, M. Muhler, S. Jobic, R. Brec, J. Rouxel, J. Solid State Chem. 121 (1996) 87.
[32] E. Canadell, S. Jobic, R. Brec, J. Rouxel, M.-H. Whangbo, J. Solid State Chem. 99 (1992) 189.